PHYSICS

Interleaved atom interferometry for high-sensitivity inertial measurements

D. Savoie*, M. Altorio*, B. Fang, L. A. Sidorenkov, R. Geiger†, A. Landragin

Cold-atom inertial sensors target several applications in navigation, geoscience, and tests of fundamental physics. Achieving high sampling rates and high inertial sensitivities, obtained with long interrogation times, represents a challenge for these applications. We report on the interleaved operation of a cold-atom gyroscope, where three atomic clouds are interrogated simultaneously in an atom interferometer featuring a sampling rate of 3.75 Hz and an interrogation time of 801 ms. Interleaving improves the inertial sensitivity by efficiently averaging vibration noise and allows us to perform dynamic rotation measurements in a so far unexplored range. We demonstrate a stability of 3×10^{-10} rad s^{-1}, which competes with the best stability levels obtained with fiber-optic gyroscopes. Our work validates interleaving as a key concept for future atom-interferometry sensors probing time-varying signals, as in onboard navigation and gravity gradiometry, searches for dark matter, or gravitational wave detection.

INTRODUCTION

Quantum sensing relies on the manipulation of internal or external degrees of freedom in atoms, molecules, optomechanical devices, and photonic or solid-state systems and covers various applications such as magnetometry (*1*–*3*), the definition of frequency standards (*4*, *5*), short-range force measurements (*6*), or electromagnetic measurements (*7*, *8*). Inertial sensors based on the coherent manipulation of superpositions of momentum states in atom interferometers have been developed for more than 25 years (*9*–*11*), with the goal of addressing various applications. Examples of remarkable achievements are tests of fundamental physics (*12*–*16*), metrology (*17*), or absolute gravimetry (*18*–*21*). These precision measurements of gravito-inertial effects directly take benefit from the inherent accuracy and long-term stability of cold-atom sensors. These two properties can eventually be combined with the high bandwidth of relative sensors, which is at the basis of sensor fusion (*22*). This approach is reminiscent of atomic clocks, where probing the stable atomic energy structure is used for stabilizing a microwave or optical oscillator (*4*, *5*) or for tests of fundamental physics.

The extension of applications of cold-atom inertial sensors to measurement of time-varying signals has been challenged by their reduced sampling rate, which originates from their sequential operation and from the long interrogation time of the atoms that is required to achieve high inertial sensitivity. This limitation is, for example, an obstacle for applications to inertial navigation (*23*) or to fundamental research related to dark matter detection (*24*) or gravitational wave astronomy (*25*, *26*). In this study, we report on the interleaved operation of a cold-atom inertial sensor, which operates with a sampling frequency of 3.75 Hz and features a high inertial sensitivity, as given by the 801-ms interrogation time of the atoms in the interferometer. The method of interleaving, which we demonstrate for both static and dynamic rotation rate measurements, can be generalized to other atom interferometer architectures and therefore paves the way to the development of high-bandwidth and high-sensitivity cold-atom inertial sensors.

Besides an increase in sensor bandwidth, we show that interleaving allows us to efficiently average vibration noise (as $1/\tau$, where τ is the integration time), which represents the most important noise source in cold-atom inertial sensors. As a consequence, we demonstrate a record rotation rate sensitivity of 3×10^{-8} rad s^{-1} $Hz^{-1/2}$. Such a high-sensitivity level allows us to characterize the systematic effects of a cold-atom gyroscope in a so far unexplored range (*27*, *28*) and to stabilize them at the few 10^{-10} rad s^{-1} level. Previous research on atomic beam gyroscopes has already demonstrated excellent sensitivities (*29*) and long-term stabilities close to the state-of-the-art optical gyroscopes (*30*). As the long-term instability of gyroscopes is a limiting factor in inertial navigation systems, achieving the performance of the best fiber-optic gyroscopes (*31*) was a long-standing goal, which we attain for the first time with a cold-atom sensor.

RESULTS

Experimental setup

Experimental sequence and principle of the gyroscope

The core of the experimental setup used in this work has been described in (*32*) and is sketched in Fig. 1. The essential techniques are given in Materials and Methods, with further details in the Supplementary Materials. In short, we laser-cool cesium atoms to a temperature of 1.2 μK and launch them vertically at a velocity of 5.0 m s^{-1}. After a selection step of the $m_F = 0$ magnetic sublevel, we interrogate the atoms in the interferometer and finally detect their state at the output of the interferometer, on their way down, using fluorescence detection. We realize the light-pulse atom interferometer using two-photon stimulated Raman transitions with counter-propagating laser beams, which couple the $|F = 3, m_F = 0\rangle$ and $|F = 4, m_F = 0\rangle$ clock states of the cesium atom.

According to the Sagnac effect, the rotation sensitivity is proportional to the area between the two arms of the interferometer. Our gyroscope is based on a fountain configuration with four light pulses to create a folded geometry owing to gravity (*33*). The symmetric four-pulse fountain configuration allows us to achieve a large area (11 cm^2 in this work) and leads to a vanishing sensitivity to constant linear accelerations. The interferometer phase shift, Φ, can be calculated from the relative phase between the two Raman lasers, $\Delta\varphi_{laser}(t) = \vec{k}_{eff} \cdot \vec{r}_{b,t}(t) + \Delta\varphi(t)$, which is imprinted on the diffracted part of the matter wave at the time t of the pulse. It reads

$$\Phi = \vec{k}_{eff} \cdot \left[\vec{r}_b(0) - 2\vec{r}_t\left(\frac{T}{2}\right) + 2\vec{r}_t\left(\frac{3T}{2}\right) - \vec{r}_b(2T) \right] + \Delta\Phi^0 \quad (1)$$

LNE-SYRTE, Observatoire de Paris, Université PSL, CNRS, Sorbonne Université, 61 Avenue de l'Observatoire, 75014 Paris, France.
*These authors contributed equally to this work.
†Corresponding author. Email: remi.geiger@obspm.fr.

where $\vec{k}_{\mathrm{eff}}$ is the two-photon wave vector, $\vec{r}_{\mathrm{b,t}}(t)$ is the position of the mirror retroreflecting the Raman lasers with respect to the center of mass of the free-falling atoms (subscripts {b, t} for bottom and top mirror; see Fig. 1), and $2T$ is the total interrogation time. The last term $\Delta\Phi^0$ is a controllable laser phase shift independent of inertial effects. The phase shift associated to the stationary Earth rotation rate $\vec{\Omega}_{\mathrm{E}}$ is given by

$$\Phi_{\Omega} = \frac{1}{2}\vec{k}_{\mathrm{eff}}\cdot(\vec{g}\times\vec{\Omega}_{\mathrm{E}})T^3 \qquad (2)$$

where $\vec{g}$ is the acceleration of gravity (*34*).

Interleaved operation

We use a sequence of joint interrogation of successive interferometers, which is obtained by using the same π/2 Raman pulse for the atom clouds entering and exiting the interferometer zone (*32*). Consequently, the sensor can operate without dead times. The interleaved operation, which is reminiscent from the atom juggling technique of (*35*), is then implemented by extending this joint sequence to a multiple-joint sequence, as proposed in (*36*). The sequence of Raman pulses is given in Fig. 1. If we denote $2T = 801$ ms as the total duration of the interferometer, then we launch an atom cloud every $T_c = 2T/3 = 267$ ms, which supposes that a cloud is laser cooled while three previously launched clouds are interrogated in the interferometer. Because of timing constraints, the loading time of the magneto-optical trap (MOT) is limited. The atoms are loaded in the MOT during 55 ms, and we detect 2×10^5 atoms at the end of the interferometer. The light scattered from the MOT atoms causes incoherent photon absorption and emission from the interrogated atoms and therefore a loss of contrast (*36*). The contrast of the interferometer is 7.4%, limited by the expansion of the cloud during the free fall in the Raman beams of Gaussian profile and by the light scattered from the MOT.

Technical upgrades

We implemented several key upgrades of our setup compared to (*32*). First, we improved the detection noise, which was limiting the sensitivity in (*32*). The equivalent one-shot phase noise is now 71 mrad, corresponding to a rotation noise of 8 nrad $\mathrm{s}^{-1}\,\mathrm{Hz}^{-1/2}$. Second, we implemented a real-time compensation of linear acceleration noise (*22*) and a servo loop to operate the interferometer at mid-fringe, i.e., in its linear range. These techniques are described in Materials and Methods. These upgrades result in a sensor that effectively operates without dead times, as statistically very few points sit on the top or bottom of a fringe, where the sensitivity vanishes.

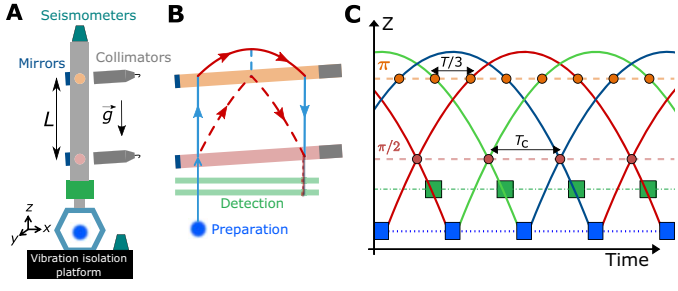

Fig. 1. Principle of the experiment. (**A**) Sketch of the experiment, where the atoms are laser cooled (blue cloud) and launched vertically, interrogated by two Raman beams (brought from the gray collimators and retroreflected on the blue mirrors), and detected on their way down (green box). The distance between the Raman beams is $L = \frac{3}{8}gT^2 \simeq 59$ cm. (**B**) Diagram of the atom interferometer in the (*xz*) plane (not to scale), with the blue and red lines labeling the $|\vec{0}\rangle$ and $\hbar\vec{k}_{\mathrm{eff}}$ momentum states, respectively. The dashed and plain lines show the two paths of the matter waves in the interferometer, which enclose an area of 11 cm^2. (**C**) Trajectories of the successively launched atom clouds in interleaved operation. Each interferometer has an interrogation time $2T = 801$ ms, and the cycle time is $T_c = 2T/3 = 267$ ms. The π/2 pulses are shared between the atom clouds entering and exiting the interferometer.

Rotation rate acquisition

Figure 2 shows a 32.5-hour acquisition of rotation rate measurements obtained between 23 and 25 September 2017. To obtain this series of data, we alternated the direction of the Raman wave vector ($\pm\vec{k}_{\mathrm{eff}}$) and computed the half-difference of two successive measurements to reject noninertial ($\vec{k}_{\mathrm{eff}}$-independent) effects, such as AC Stark shifts (see Materials and Methods and section S1 for the details of the sequence and section S2 for the raw data). In the following, we will analyze the sensitivity and the stability of the gyroscope from this acquisition.

Efficient averaging of vibration noise and record sensitivity

Vibration noise is the most important source of sensitivity degradation in cold-atom inertial sensors of large area [i.e., using long interrogation time and/or large momentum transfer techniques (*37*)]. Efficient vibration isolation at low frequencies (below a few hertz) is technically challenging [e.g., (*38*)] and not suited for field applications. We will show that interleaving allows us to reduce the impact of this key noise source.

In our sensor, the impact of inertial noise can be analyzed by considering a center of rotation located at the top Raman beam: Inertial noise then appears as linear acceleration noise of both mirrors plus rotation noise of the bottom mirror. The rotation noise translates into random variations of the angle $\theta_{\mathrm{B}}(t)$ of the Raman beam with respect to a geostationary reference frame (*34*) and affects the interferometer phase as $[\theta_{\mathrm{B}}(2T) - \theta_{\mathrm{B}}(0)]$ (Eq. 1). In joint measurements, in which π/2 pulses are shared (occurring at times 0 and $2T$), the contribution of rotation noise cancels out when averaging N successive measurements (see Materials and Methods for a derivation). Therefore, the gyroscope sensitivity should improve as τ^{-1}, where $\tau = 2NT$ is the integration time, instead of $\tau^{-1/2}$ in the case of uncorrelated measurements affected by rotation noise.

Besides averaging rotation noise, the interleaved operation of our sensor allows us to reduce the impact of residual linear acceleration noise: Because our sampling frequency ($1/T_c = 3.75$ Hz) is higher than the frequencies at which the acceleration noise mostly contributes (around 0.5 Hz; see table S1), correlations appear between successive

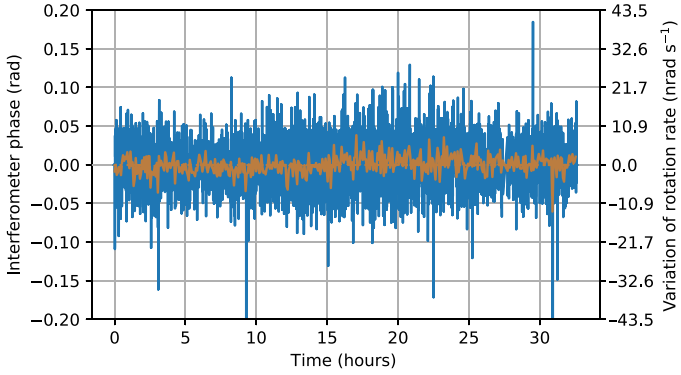

Fig. 2. Rotation rate measurement during 32.5 hours. In the blue (orange) trace, each data point is the average over segments of 26.7 s (267 s) of raw inertial phase measurements. The right axis translates inertial phase to rotation rate using the scale factor of the gyroscope to stationary Earth rotation (from Eq. 2).

measurements, yielding a scaling of the sensitivity that approaches τ^{-1} (rather than $\tau^{-1/2}$).

Figure 3 shows the Allan deviation of the gyroscope stability for an 11.3-hour portion of night data of Fig. 2. The improvement of the sensitivity as τ^{-1} for integration times up to $\simeq 7$ s is clear. The stability then gradually enters the $\tau^{-1/2}$ regime characteristic of uncorrelated white noise, corresponding to a sensitivity of 3×10^{-8} rad s^{-1} Hz$^{-1/2}$. This sensitivity, which improves by more than a factor of 3 on our previous result (*32*), establishes the new record for cold-atom gyroscopes. As a comparison, our short-term sensitivity competes favorably with that of the best fiber-optic gyroscopes (*31*). This sensitivity enables us to study several systematic effects affecting a cold-atom gyroscope for the first time in the range of low 10^{-9} rad s^{-1}.

Systematic effects and gyroscope long-term stability

A systematic shift specific to the interleaved interrogation originates from the light scattered from the MOT toward the atoms interrogated in the interferometer (*36*). The MOT scattered light is close to resonance and induces a loss of contrast and a differential light shift (AC Stark shift). The influence of induced light shifts is reduced by the spin-echo–like four-pulse sequence and by the use of $\vec{k}_{\mathrm{eff}}$ reversal: Alternating $\pm\hbar\vec{k}_{\mathrm{eff}}$ momentum transfers changes the sign of the inertial phase shift but not the one of the clock terms (e.g., differential light shift), which are rejected when taking the half-difference of two measurements (as done in Fig. 2). We measured the residual effect and showed that it corresponds to an instability below 7×10^{-11} rad s^{-1} (see Supplementary Materials). Although currently negligible, this effect is purely technical and could be resolved by having the MOT and the detection region out of view from the atom interferometer region in future designs.

The most important systematic effects in atom interferometers with separated Raman beams originate from relative wavefront mismatch coupled to deviations of the atom trajectories with respect to the ideal one (*27*, *39*). In our system, a relative angular misalignment $\vec{\delta}\theta$ between the top and bottom mirrors used to retroreflect the Raman beams (Fig. 1), coupled with an error of launch velocity $\vec{\delta}v$ (with respect to a velocity of $-\vec{g}T$ at the first Raman pulse) in the (y, z) plane, results in a phase shift

$$\begin{aligned}\Delta\Phi &= 2Tk_{\mathrm{eff}}(\delta v_y \delta\theta_y + \delta v_z \delta\theta_z) \\ &= 12\mathrm{mrad} \times \left(\frac{\delta v_{y,z}}{1\mathrm{mm.s}^{-1}}\right) \times \left(\frac{\delta\theta_{y,z}}{1\mu\mathrm{rad}}\right) \end{aligned} \quad (3)$$

We explain in Materials and Methods how we set the parallelism between the two Raman beams and the velocity of the atoms to approach the ideal trajectory to achieve an uncertainty on the residual systematic shift of 21 mrad (i.e., 4.6 nrad s^{-1}, from Eq. 2).

After this systematic analysis and the corresponding fine-tuning of the apparatus, we recorded the rotation rate acquisition displayed on Fig. 2. The stability of the gyroscope over the entire acquisition is analyzed in the Supplementary Materials (fig. S5) and is in agreement with that read from Fig. 3 for shorter integration times.

Dynamic rotation rate measurements

We use the unprecedented sampling rate and inertial sensitivity of our gyroscope to perform measurements of weak dynamic rotation rates. To this end, we modulate the orientation of the experiment around the y axis. This was performed by applying a force on the bottom plate linking the experimental frame to the vibration isolation platform via the voice-coil actuator controlling the tilt θ_x of the apparatus. We apply sinusoidal modulations of the form $\theta_x(t) = \theta_0 \sin(\omega t)$ with a period $2\pi/\omega$ and with an amplitude θ_0 of a few 10^{-7} rad. The resulting rotation rate is of the form $\vec{\Omega}(t) = \Omega_0 \cos(\omega t)\hat{u}_y$, with $\Omega_0 = \omega\theta_0$. The measurements are reported in Fig. 4 for modulation periods of 5 and 10 s. The respective modulation amplitudes are 2.3×10^{-7} and 3.4×10^{-7} rad. Figure 4 (A and B) shows the atomic phase extracted from the transition probability, $P(t)$, which follows the sinusoidal modulation. The total rotation signal from the atom interferometer is the sum of this atomic phase and the phase compensated in real time. A Fourier analysis of the total signal is shown in Fig. 4C. Within our frequency resolution, we find that the amplitude of the reconstructed rotation rate signal agrees with the expectation of Ω_0 with a relative precision of 5%. A more detailed analysis is presented in section S5. Our proof-of-principle experiment, performed in a so far unexplored range of time resolution and inertial sensitivity for a cold-atom sensor, demonstrates the impact of interleaved atom interferometry for dynamic measurements.

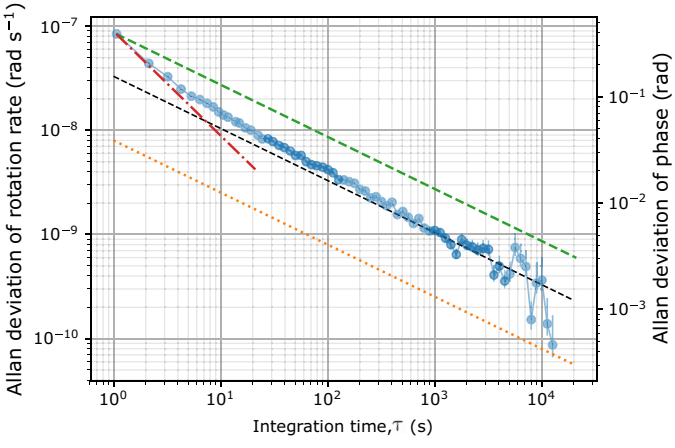

Fig. 3. Gyroscope sensitivity. Stability analysis of an 11.3-hour portion of rotation rate measurements of Fig. 2, between 1:22 a.m. and 12:47 p.m. on 24 September 2017. The error bars represent the 68% confidence intervals on the estimation of the Allan deviation. Dashed black line, 3.3×10^{-8} rad s$^{-1} \times \tau^{-1/2}$; green dashed line, $\tau^{-1/2}$ scaling from the one-shot Allan deviation; red dotted-dashed line, τ^{-1} scaling from the one-shot Allan deviation; orange dotted line, detection noise limit corresponding to 8×10^{-9} rad s$^{-1} \times \tau^{-1/2}$.

DISCUSSION

We have demonstrated the method of interleaving in a large-area atom interferometer, as a way to reach high sampling frequencies and high inertial sensitivities together. Interleaving enables us to efficiently average vibration noise (the largest noise source in cold-atom inertial sensors) and is thus a promising way of reaching the quantum projection noise limit, a necessary condition before increasing the atom flux or implementing schemes to approach the Heisenberg limit. As a result, we demonstrated record short-term sensitivities for a cold-atom gyroscope and could thus characterize systematic effects in a so far unexplored range. The rotation rate sensitivity and stability that we achieved competes with that of the best strategic-grade fiber-optic gyroscopes [long-term stability in the range of 5×10^{-10} rad s^{-1} (*31*)]. Our results thus pave the way for a change of technology in future high-precision inertial navigation systems.

In our setup, the maximum number of interleaved measurements is technically limited to three because of the arrangement of our detection

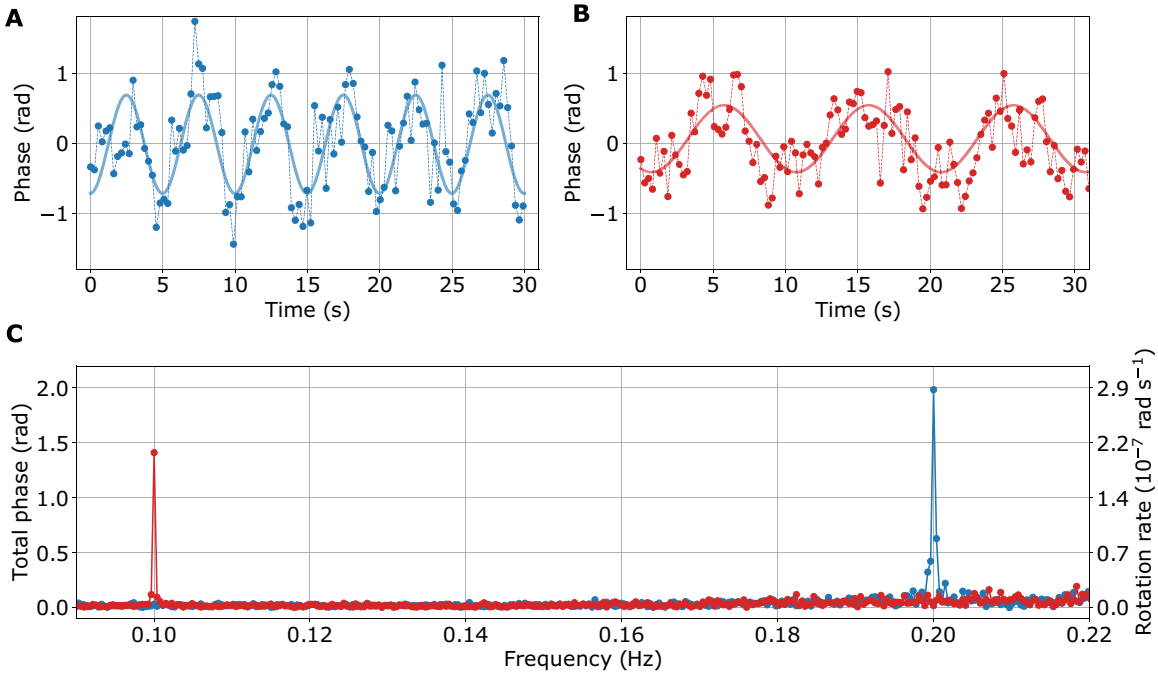

Fig. 4. Measurement of dynamic rotation rates. Atom interferometer phase deduced from the transition probability, for rotation rate modulations of 5-s period (**A**) and 10-s period (**B**). Plain line, sinusoidal fit to guide the eye. (**C**) Fourier analysis of the total rotation rate signal, with a frequency resolution of 0.37 mHz.

system with respect to the MOT region (see Materials and Methods). In a dedicated design, e.g., where the detection region would be out of view from the upcoming clouds, sampling frequencies of 20 Hz or higher could be reached. As an alternative, the use of atoms characterized by different transition wavelengths for the cooling/detection/atom interferometer would be beneficial to circumvent the effects associated with the scattered light from the source or the detected atoms. Our technique is thus well suited for ongoing developments of atom interferometers with alkaline-earth atoms (*40*).

Interleaving ties well with laser-cooling techniques, which are able to rapidly (in less than 100 ms) produce cold samples with more than 10^7 atoms. Laser cooling beyond optical molasses such as degenerate Raman sideband cooling appears as a suitable solution for an increased brightness without compromising the cycling frequency. Interleaving is, in principle, also compatible with the production of ultracold, collimated, atom sources (*16*), provided that they can be produced (*41*) or extracted at sufficiently high (several hertz) repetition rates.

The method of interleaved atom interferometry can be applied to different sensor architectures, such as multi-axis accelerometers (by alternating measurements along different axes at a high repetition rate), gavimeters, or gradiometers. For example, interleaving can be exploited to realize a gravimeter of both high accuracy and high sensitivity in a single instrument, potentially allowing to surpass superconducting gravimeters that currently feature record sensitivities but require regular calibrations. Hence, interleaving is representative of the flexibility of cold atoms for realizing versatile inertial sensors, as compared to architectures involving macroscopic masses and electromechanical systems. Regarding fundamental physics applications, achieving high sampling rates is a prerequisite for future studies on dark matter with atomic accelerometers (*24*), as well as for gravitational wave detection with atom interferometers (*25*, *26*). Interleaving is therefore a key concept for future applications of cold-atom inertial sensors.

MATERIALS AND METHODS

Details of the experiment

Cesium atoms loaded from a two-dimensional (2D) MOT were trapped and laser cooled in a 3D MOT. We launched the atoms vertically at a velocity of 5.0 m s^{-1} using moving molasses with a (3D) cloud temperature of 1.2 μK. After the MOT and before the interrogation, the atoms were prepared in the $|F = 4, m_F = 0\rangle$ state using a selection scheme based on the Stern-Gerlach effect (magnetic deflection of the atoms in $m_F \neq 0$ states). Light pulse interferometry is realized using two phase-locked Raman lasers that couple the cesium clock states (hyperfine splitting of 9.192 GHz). The Raman lasers have a wavelength close to the D_2 line (wavelength $\lambda \simeq 852$ nm) and are detuned by 470 MHz from the excited state to reduce incoherent scattering. The impact of residual relative Raman laser phase noise has been estimated to 50 mrad per shot of atom interferometer phase. The Raman lasers were sent to the atoms through two optical windows separated by $L = \frac{3}{8} g T^2 \simeq 59$ cm, with an interrogation time $2T = 801$ ms. We used Gaussian Raman beams with $1/e^2$ diameter equal to 40 mm and about 120 mW of total power. The interferometer output signal was determined by the probability of transition, P, from the $F = 4$ to the $F = 3$ state, which is read out via fluorescence detection of the two levels' populations after the atom interferometer light-pulse sequence. The probability of transition was modulated according to $P = P_0 + A \sin \Phi$, where $C = 2A$ is the interferometer contrast and Φ is the interferometer phase.

Our experiment uses retroreflected Raman beams, such as to form two pairs of Raman beams inducing two transitions: one in the $+\vec{k}_{\text{eff}}$ direction and another in the $-\vec{k}_{\text{eff}}$ direction. Selectivity of the $\pm\vec{k}_{\text{eff}}$ transitions is provided by tilting the Raman beams by an angle $\theta \simeq 3.80°$ with respect to the horizontal to introduce a Doppler shift ($\pm k_{\text{eff}} g T \sin \theta / 2\pi \simeq \pm 611$ kHz at the first and last $\pi/2$ pulses), which is much larger than the width of the atom Doppler distribution (~ 40 kHz). To follow the resonance condition at each Raman pulse, we stepwise

changed the relative frequency between the two Raman lasers during the sequence, to match the values given by the underlying frequency chirp pattern (see details in fig. S2). To apply the frequency steps, we used a direct digital synthesizer driven by an FPGA (field-programmable gate array).

Real-time compensation of vibration noise and mid-fringe lock

We measured the vibrations of the setup with two broadband seismometers (model Trillium Compact 120 s from Nanometrics) located at the bottom and top of the experimental frame (see Fig. 1). From the measured signal, we estimated the interferometer phase shift due to vibrations and applied a corresponding phase jump to the relative phase of the Raman lasers 15 ms before the last pulse. This allows us to reduce the standard deviation (SD) of the interferometer phase from about 3.2 to 0.5 rad. To work within the linear regime where the sensitivity is maximal, we alternated measurements on both sides of a fringe and computed an error signal from two successive measurements of the transition probability. This error signal was integrated and used to servo-lock the interferometer at mid-fringe via a feedback on the Raman laser relative phase. More details are given in section S1.

Efficient averaging of vibration noise

Following Eq. 1 and assuming that the Raman lasers are oriented purely in the x direction, the four-light-pulse atom interferometer phase shift is given by (we neglect the duration of the Raman pulse)

$$\Phi = k_{\mathrm{eff}}[x_{\mathrm{b}}(0) - 2x_{\mathrm{t}}(T/2) + 2x_{\mathrm{t}}(3T/2) - x_{\mathrm{b}}(2T)] \quad (4)$$

with $x_{\mathrm{b,t}}(t)$ as the position of the bottom and top retro-mirrors with respect to the free-falling atom cloud. The phase shift can be rewritten as

$$\begin{aligned}\Phi &= k_{\mathrm{eff}}[x_{\mathrm{t}}(0) - 2x_{\mathrm{t}}(T/2) + 2x_{\mathrm{t}}(3T/2) - x_{\mathrm{t}}(2T)] \\ &\quad + k_{\mathrm{eff}}([x_{\mathrm{b}}(0) - x_{\mathrm{t}}(0)] - [x_{\mathrm{b}}(2T) - x_{\mathrm{t}}(2T)]) \\ &= \Phi_{\mathrm{t}}^{\mathrm{acc}} + k_{\mathrm{eff}} L(\theta_{\mathrm{b}}(0) - \theta_{\mathrm{b}}(2T)) \end{aligned} \quad (5)$$

with $L = \frac{3}{8} g T^2$ as the distance between the bottom and top mirrors and Φ_t^{acc} as the term associated to the linear acceleration of the top mirror. The second term represents pure rotation of the bottom mirror about the position of the top one. Recalling that $T_{\mathrm{c}} = 2T/3$ and writing as $\Phi_i = \Phi(iT_{\mathrm{c}})$ the atom interferometer phase at cycle i, the mean phase after N measurement reads

$$\begin{aligned}\bar{\Phi}_N = \frac{1}{N}\sum_{i=0}^{N-1}\Phi_i = \frac{1}{N}\sum_{i=0}^{N-1}(k_{\mathrm{eff}} L[\theta_{\mathrm{b}}(iT_{\mathrm{c}}) - \theta_{\mathrm{b}}((i+3)T_{\mathrm{c}})] \\ + \delta\tilde{\phi}_i)\end{aligned} \quad (6)$$

The term $\delta\tilde{\phi}_i$ encompasses contributions of detection noise, uncompensated linear acceleration noise, and laser phase noise. When expanding the sum in Eq. 6, most of the θ_{b} terms mutually cancel such that the mean phase reads

$$\bar{\Phi}_N = k_{\mathrm{eff}} L \frac{\theta_{\mathrm{b}}(0) - \theta_{\mathrm{b}}((N+2)T_{\mathrm{c}})}{N} + \frac{1}{N}\sum_{i=0}^{N-1}\delta\tilde{\phi}_i \quad (7)$$

This equation shows that the random rotation noise averages as N^{-1} (first term). The second term represents the uncorrelated noise contributions of SD $\sigma_{\delta\phi}$. Their sum equals $\sqrt{N} \times \sigma_{\delta\phi}$, which corresponds to a scaling of the phase sensitivity as $N^{-1/2}$.

Besides rotation noise, uncompensated linear accelerations in the frequency range [0.1 – 1] Hz contribute, to a large part, to the interferometer phase noise (see section S3 for details). This contribution, estimated to typically about 500 mrad per shot, dominates the noise budget and may prevent from observing a clear τ^{-1} scaling of the gyroscope sensitivity. Interleaving, however, allows us to oversample these fluctuations, thus introducing correlations between successive measurements, which also contribute to the τ^{-1} dependence of the instrument sensitivity.

Alignment of the two Raman beams and atom trajectory

We set the parallelism between the top and bottom Raman beams by means of a two-axis piezo-motorized mirror mount with a resolution of 0.7 μrad. By optimizing the contrast of the interferometer, we approached the parallelism with an uncertainty of about 3 μrad, which is required for the matter waves to recombine at the output of the interferometer. For the fine adjustment, we measured the dependence of the phase shift of Eq. 3, $\Delta\Phi = 2Tk_{\mathrm{eff}}(\delta v_y \delta\theta_y + \delta v_z \delta\theta_z)$, on $\delta\theta_{y,z}$ and $\delta v_{y,z}$ (as defined in the main text). To this end, we set the atom trajectory in the (y, z) directions by varying the tilt of the experiment (y direction) and the launch velocity during the moving molasses phase (z direction). In the z direction, we could zero the systematic effect with an uncertainty of 5 mrad. This amounts to set the velocity of the atoms at the first Raman pulse to the ideal velocity ($v_z = gT$) with an uncertainty of 0.6 mm s^{-1} and to set the parallelism between two mirrors in the z direction with an uncertainty of 0.7 μrad.

The minimization of the systematic shift in the y direction was technically more difficult to achieve than in the z direction: recording the dependence of the phase shift on $\delta\theta_y$ for various velocities required to tilt the entire apparatus by several mrad to vary δv_y by several mm s^{-1}. This procedure required to manually move masses on the base plate of the experiment sitting on a floating vibration isolation platform, which introduced instabilities. We managed to set the y velocity close to the ideal velocity ($v_y = 0$) with an uncertainty of 1.8 mm s^{-1}. The residual shift corresponds to a phase variation of 21 mrad per microradian of $\delta\theta_y$ variation.

Limitation to the number of interleaved interferometers

When trying five interleaved cycles, we observed a marked loss of contrast of the interferometer. The reason is that when a (descending) atom cloud at the output of the interferometer enters the detection region, a part of the light scattered by the atoms is directed toward the (ascending) cloud, which optically pumps atoms to unwanted magnetic states and heats them before they enter the interferometer.

SUPPLEMENTARY MATERIALS

Supplementary material for this article is available at http://advances.sciencemag.org/cgi/content/full/4/12/eaau7948/DC1

Section S1. Real-time compensation of vibration noise, mid-fringe lock, and details of the sequence
Section S2. Raw data
Section S3. Analysis of vibration noise
Section S4. Stability analysis
Section S5. Analysis of the dynamic rotation rate measurements
Section S6. Systematic effect from the scattered light
Fig. S1. Histogram of the vibration phase and of the interferometer phase with real-time compensation of vibration.
Fig. S2. Details of the sequence.
Fig. S3. Raw interferometer measurements corresponding to the data presented in Fig. 2.

Fig. S4. Analysis of vibration noise.
Fig. S5. Stability analysis of the gyroscope.
Table S1. Contribution of the linear acceleration noise to the interferometer phase noise by frequency band.
Reference (*42*)

REFERENCES AND NOTES

1. D. Sheng, S. Li, N. Dural, M. V. Romalis, Subfemtotesla scalar atomic magnetometry using multipass cells. *Phys. Rev. Lett.* **110**, 160802 (2013).
2. I. Gross, W. Akhtar, V. Garcia, L. J. Martínez, S. Chouaieb, K. Garcia, C. Carrétéro, A. Barthélémy, P. Appel, P. Maletinsky, J.-V. Kim, J. Y. Chauleau, N. Jaouen, M. Viret, M. Bibes, S. Fusil, V. Jacques, Real-space imaging of non-collinear antiferromagnetic order with a single-spin magnetometer. *Nature* **549**, 252–256 (2017).
3. R. Jiménez-Martínez, J. Kołodyński, C. Troullinou, V. G. Lucivero, J. Kong, M. W. Mitchell, Signal tracking beyond the time resolution of an atomic sensor by Kalman filtering. *Phys. Rev. Lett.* **120**, 040503 (2018).
4. M. Takamoto, F.-L. Hong, R. Higashi, H. Katori, An optical lattice clock. *Nature* **435**, 321–324 (2005).
5. R. Le Targat, L. Lorini, Y. Le Coq, M. Zawada, J. Guéna, M. Abgrall, M. Gurov, P. Rosenbusch, D. G. Rovera, B. Nagórny, R. Gartman, P. G. Westergaard, M. E. Tobar, M. Lours, G. Santarelli, A. Clairon, S. Bize, P. Laurent, P. Lemonde, J. Lodewyck, Experimental realization of an optical second with strontium lattice clocks. *Nat. Commun.* **4**, 2109 (2013).
6. M. G. Tarallo, T. Mazzoni, N. Poli, D. V. Sutyrin, X. Zhang, G. M. Tino, Test of einstein equivalence principle for 0-spin and half-integer-spin atoms: Search for spin-gravity coupling effects. *Phys. Rev. Lett.* **113**, 023005 (2014).
7. T. Bagci, A. Simonsen, S. Schmid, L. G. Villanueva, E. Zeuthen, J. Appel, J. M. Taylor, A. Sørensen, K. Usami, A. Schliesser, E. S. Polzik, Optical detection of radio waves through a nanomechanical transducer. *Nature* **507**, 81–85 (2014).
8. A. Facon, E.-K. Dietsche, D. Grosso, S. Haroche, J.-M. Raimond, M. Brune, S. Gleyzes, A sensitive electrometer based on a Rydberg atom in a Schrödinger-cat state. *Nature* **535**, 262–265 (2016).
9. Ch. J. Bordé, Atomic interferometry with internal state labelling. *Phys. Lett. A* **140**, 10–12 (1989).
10. M. Kasevich, S. Chu, Atomic interferometry using stimulated Raman transitions. *Phys. Rev. Lett.* **67**, 181–184 (1991).
11. F. Riehle, Th. Kisters, A. Witte, J. Helmcke, Ch. J. Bordé, Optical Ramsey spectroscopy in a rotating frame: Sagnac effect in a matter-wave interferometer. *Phys. Rev. Lett.* **67**, 177–180 (1991).
12. R. Bouchendira, P. Cladé, S. Guellati-Khélifa, F. Nez, F. Biraben, New determination of the fine structure constant and test of the quantum electrodynamics. *Phys. Rev. Lett.* **106**, 080801 (2011).
13. S. Lepoutre, A. Gauguet, G. Trénec, M. Büchner, J. Vigué, He-Mckellar-Wilkens topological phase in atom interferometry. *Phys. Rev. Lett.* **109**, 120404 (2012).
14. L. Zhou, S. Long, B. Tang, X. Chen, F. Gao, W. Peng, W. Duan, J. Zhong, Z. Xiong, J. Wang, Y. Zhang, M. Zhan, Test of equivalence principle at 10^{-8} level by a dual-species double-diffraction Raman atom interferometer. *Phys. Rev. Lett.* **115**, 013004 (2015).
15. M. Jaffe, P. Haslinger, V. Xu, P. Hamilton, A. Upadhye, B. Elder, J. Khoury, H. Müller, Testing sub-gravitational forces on atoms from a miniature in-vacuum source mass. *Nat. Phys.* **13**, 938–942 (2017).
16. P. Asenbaum, C. Overstreet, T. Kovachy, D. D. Brown, J. M. Hogan, M. A. Kasevich, Phase shift in an atom interferometer due to spacetime curvature across its wave function. *Phys. Rev. Lett.* **118**, 183602 (2017).
17. G. Rosi, F. Sorrentino, L. Cacciapuoti, M. Prevedelli, G. M. Tino, Precision measurement of the Newtonian gravitational constant using cold atoms. *Nature* **510**, 518–521 (2014).
18. A. Peters, K. Y. Chung, S. Chu, High-precision gravity measurements using atom interferometry. *Metrologia* **38**, 25 (2001).
19. C. Freier, M. Hauth, V. Schkolnik, B. Leykauf, M. Schilling, H. Wziontek, H.-G. Scherneck, J. Müller, A. Peters, Mobile quantum gravity sensor with unprecedented stability. *J. Phys. Conf. Ser.* **723**, 012050 (2016).
20. Y. Bidel, N. Zahzam, C. Blanchard, A. Bonnin, M. Cadoret, A. Bresson, D. Rouxel, M. F. Lequentrec-Lalancette, Absolute marine gravimetry with matter-wave interferometry. *Nat. Commun.* **9**, 627 (2018).
21. R. Karcher, A. Imanaliev, S. Merlet, F. Pereira Dos Santos, Improving the accuracy of atom interferometers with ultracold sources. *New J. Phys.* **20**, 113041 (2018).
22. J. Lautier, L. Volodimer, T. Hardin, S. Merlet, M. Lours, F. Pereira Dos Santos, A. Landragin, Hybridizing matter-wave and classical accelerometers. *Appl. Phys. Lett.* **105**, 144102 (2014).
23. C. Jekeli, Navigation error analysis of atom interferometer inertial sensor. *Navigation* **52**, 1–14 (2005).
24. P. W. Graham, D. E. Kaplan, J. Mardon, S. Rajendran, W. A. Terrano, Dark matter direct detection with accelerometers. *Phys. Rev. D* **93**, 075029 (2016).
25. W. Chaibi, R. Geiger, B. Canuel, A. Bertoldi, A. Landragin, P. Bouyer, Low frequency gravitational wave detection with ground-based atom interferometer arrays. *Phys. Rev. D* **93**, 021101 (2016).
26. P. W. Graham, J. M. Hogan, M. A. Kasevich, S. Rajendran, Resonant mode for gravitational wave detectors based on atom interferometry. *Phys. Rev. D* **94**, 104022 (2016).
27. A. Gauguet, B. Canuel, T. Lévèque, W. Chaibi, A. Landragin, Characterization and limits of a cold-atom Sagnac interferometer. *Phys. Rev. A* **80**, 063604 (2009).
28. P. Berg, S. Abend, G. Tackmann, C. Schubert, E. Giese, W. P. Schleich, F. A. Narducci, W. Ertmer, E. M. Rasel, Composite-light-pulse technique for high-precision atom interferometry. *Phys. Rev. Lett.* **114**, 063002 (2015).
29. T. L. Gustavson, A. Landragin, M. A. Kasevich, Rotation sensing with a dual atom-interferometer Sagnac gyroscope. *Class. Quantum Gravity* **17**, 2385 (2000).
30. D. S. Durfee, Y. K. Shaham, M. A. Kasevich, Long-term stability of an area-reversible atom-interferometer Sagnac gyroscope. *Phys. Rev. Lett.* **97**, 240801 (2006).
31. H. C. Lefèvre, The fiber-optic gyroscope, a century after Sagnac's experiment: The ultimate rotation-sensing technology? *C. R. Phys.* **15**, 851–858 (2014); for recent performances, see, e.g., iXblue ultimate-performance Fiber-Optic Gyroscope (FOG) (http://web.ixblue.com/cn/aw6ym/fiberoptic-gyroscope).
32. I. Dutta, D. Savoie, B. Fang, B. Venon, C. L. Garrido Alzar, R. Geiger, A. Landragin, Continuous cold-atom inertial sensor with 1 nrad / sec rotation stability. *Phys. Rev. Lett.* **116**, 183003 (2016).
33. B. Canuel, F. Leduc, D. Holleville, A. Gauguet, J. Fils, A. Virdis, A. Clairon, N. Dimarcq, Ch. J. Bordé, A. Landragin, P. Bouyer, Six-axis inertial sensor using cold-atom interferometry. *Phys. Rev. Lett.* **97**, 010402 (2006).
34. J. K. Stockton, K. Takase, M. A. Kasevich, Absolute geodetic rotation measurement using atom interferometry. *Phys. Rev. Lett.* **107**, 133001 (2011).
35. R. Legere, K. Gibble, Quantum scattering in a juggling atomic fountain. *Phys. Rev. Lett.* **81**, 5780–5783 (1998).
36. M. Meunier, I. Dutta, R. Geiger, C. Guerlin, C. L. Garrido Alzar, A. Landragin, Stability enhancement by joint phase measurements in a single cold atomic fountain. *Phys. Rev. A* **90**, 063633 (2014).
37. S. M. Dickerson, J. M. Hogan, A. Sugarbaker, D. M. S. Johnson, M. A. Kasevich, Multiaxis inertial sensing with long-time point source atom interferometry. *Phys. Rev. Lett.* **111**, 083001 (2013).
38. J. M. Hensley, A. Peters, S. Chu, Active low frequency vertical vibration isolation. *Rev. Sci. Instrum.* **70**, 2735–2741 (1999).
39. G. Tackmann, P. Berg, C. Schubert, S. Abend, M. Gilowski, W. Ertmer, E. M. Rasel, Self-alignment of a compact large-area atomic Sagnac interferometer. *New J. Phys.* **14**, 015002 (2012).
40. L. Hu, N. Poli, L. Salvi, G. M. Tino, Atom interferometry with the Sr optical clock transition. *Phys. Rev. Lett.* **119**, 263601 (2017).
41. J. Rudolph, W. Herr, C. Grzeschik, T. Sternke, A. Grote, M. Popp, D. Becker, H. Müntinga, H. Ahlers, A. Peters, C. Lämmerzahl, K. Sengstock, N. Gaaloul, W. Ertmer, E. M. Rasel, A high-flux BEC source for mobile atom interferometers. *New J. Phys.* **17**, 065001 (2015).
42. P. Cheinet, B. Canuel, F. Pereira Dos Santos, A. Gauguet, F. Yver-Leduc, A. Landragin, Measurement of the sensitivity function in a time-domain atomic interferometer. *IEEE Trans. Instrum. Meas.* **57**, 1141–1148 (2008).

Acknowledgments: We thank F. Pereira Dos Santos for careful reading of the manuscript. **Funding:** We acknowledge the financial support from Ville de Paris (project HSENS-MWGRAV), FIRST-TF (ANR-10-LABX-48-01), Centre National d'Etudes Saptiales (CNES), Sorbonne Universités (project SU-16-R-EMR-30, LORINVACC), and Action Spécifique du CNRS Gravitation, Références, Astronomie et Métrologie (GRAM). B.F. was funded by Conseil Scientifique de l'Observatoire de Paris, D.S. by Direction Générale de l'Armement, and M.A. by the EDPIF doctoral school. **Author contributions:** D.S., M.A., and B.F. performed the experiments, and L.A.S. contributed to the dynamic rotation rate measurements. D.S., R.G., and M.A. analyzed the data. R.G. and D.S. wrote the manuscript. A.L. conceived the experiment. R.G. and A.L. supervised the research. All authors discussed the manuscript. **Competing interests:** The authors declare that they have no competing interests. **Data and materials availability:** All data needed to evaluate the conclusions in the paper are present in the paper and/or the Supplementary Materials. Additional data related to this paper may be requested from the authors.

Submitted 17 July 2018
Accepted 19 November 2018
Published 21 December 2018
10.1126/sciadv.aau7948

Citation: D. Savoie, M. Altorio, B. Fang, L. A. Sidorenkov, R. Geiger, A. Landragin, Interleaved atom interferometry for high-sensitivity inertial measurements. *Sci. Adv.* **4**, eaau7948 (2018).

Interleaved atom interferometry for high-sensitivity inertial measurements

D. Savoie, M. Altorio, B. Fang, L. A. Sidorenkov, R. Geiger and A. Landragin

Sci Adv **4** (12), eaau7948.
DOI: 10.1126/sciadv.aau7948